

Numerical Analysis of Nanotube-Based NEMS Devices—Part I: Electrostatic Charge Distribution on Multiwalled Nanotubes

Changhong Ke

Horacio D. Espinosa¹
e-mail: espinosa@northwestern.edu

Department of Mechanical Engineering,
Northwestern University,
2145 Sheridan Road,
Evanston, IL 60208

The charge distribution on the surface of a biased conductive, finite-length, cylindrical nanotube, free standing above an infinite grounded plane, is investigated. The diameter range of the cylinder tube under study is 20–60 nm, which is much larger than the screening length, meaning the quantum and statistical effects on the charge distribution are negligible. The relationship between the charge distribution and the geometry of the nanotube is examined in detail by classical electrostatics using full three-dimensional numerical simulations based on the boundary element method. A model of the concentrated charge at the end of nanotubes is proposed. The charge distribution for a clamped cantilever nanotube is also computed and discussed. The findings here reported are of particular usefulness in the design and modeling of electrostatic actuated nanotube/nanowire based nano-electromechanical systems. [DOI: 10.1115/1.1985434]

Introduction

Carbon nanotubes (CNTs) and nanowires have received significant interest within the science community because of their unique electromechanical properties. CNTs have been used as key elements to build nano-electromechanical systems (NEMS), such as CNT-based nanotweezers, [1,2] nonvolatile random access memory, [3] nanorelays, [4] rotational actuators, [5] and feedback-controlled nanocantilever devices [6]. Likewise, Si nanowire-based devices, such as high-frequency resonators [7] and bistable nano-electromechanical devices, [8] are of particular interest because of the central role of Si in the semiconductor industry and hence the existing set of known fabrication technologies.

One of the key issues in the design of devices is the understanding of their electromechanical characteristics. Concerning its mechanical response, it has been shown that classical continuum theory is well applicable to their analysis [9]. Concerning device electrical characteristics, a detailed analysis of charge distribution on nanotubes, or nanowires, is critical to the precise calculation of electrostatic forces. Although nanotubes have hollow structures, carbon nanotubes with capped ends are more electrochemically stable than those with open ends [10]. Thus, nanotubes with finite length, as well as nanowires, can be geometrically approximated by conductive nanocylinders. For small-scale nanocylinders, the density of states on the surface is finite. The screening length, the distance that the “surface charge” actually penetrates into the cylinder interior, is found to be a nanometer scale quantity [11]. For nanocylinders with transverse dimension, i.e., diameter, approaching the screening length, such as single-walled carbon nanotube, the finite size and quantum effects have to be considered thor-

oughly when calculating the surface/volume charge distribution [12,13]. For nanocylinders with transverse dimension much larger than the screening length, such as multiwalled carbon nanotubes or nanowires with outer diameter larger than 20 nm, this quantum effect can be considered negligible. Thus, the charge distribution can be approximated by the charge distribution on a metallic, perfectly conductive cylinder with the same geometry, to which classical electrostatic analysis can be applied. This is the case under examination in the following. Because there are two types of boundary surfaces in cylindrical-shape conductors with finite length—the cylindrical side surface and the planar end surface—essentially classical distribution of charge density with a significant charge concentration at the cylinder end has been observed [13,14]. However, there is still a lack of simple models or formulas to describe the charge distribution along finite length conductive nanocylinders; in particular, the concentration of charges at the cylinder ends.

In this paper, we compute the charge distribution on a finite-length conductive nano-scale cylinder based on classical electrostatics, by employing three-dimensional (3D) numerical simulations. Two types of boundary conditions are analyzed: (i) freestanding nanotube and (ii) clamped-free end nanotube cantilever. A formula for the charge distribution including end charge effects is derived from a parametric analysis.

Electrostatic Calculation of Charge Distribution

In the following we define a full 3D model to investigate the charge distribution in a freestanding conductive nanotube of radius R and length L , which is spaced from the ground plane by a distance H . The geometry and coordinate system is schematically shown in Fig. 1.

For an infinitely long, perfectly conductive cylindrical nanotube, placed over an infinite conducting plane, the charges per unit length ρ_{L0} can be expressed as [15]

$$\rho_{L0} = \frac{2\pi\epsilon_0 V_0}{a \cosh(1 + H/R)} \quad (1)$$

where V_0 is the potential and ϵ_0 is the permittivity of vacuum ($\epsilon_0 = 8.854 \times 10^{-12} \text{ C}^2 \text{ N}^{-1} \text{ m}^{-2}$).

¹To whom correspondence should be addressed.

Contributed by the Applied Mechanics Division of THE AMERICAN SOCIETY OF MECHANICAL ENGINEERS for publication in the ASME JOURNAL OF APPLIED MECHANICS. Manuscript received by the Applied Mechanics Division, December 17, 2004; final revision, January 26, 2005. Associate Editor: R. M. McMeeking. Discussion on the paper should be addressed to the Editor, Prof. Robert M. McMeeking, Journal of Applied Mechanics, Department of Mechanical and Environmental Engineering, University of California - Santa Barbara, Santa Barbara, CA 93106-5070, and will be accepted until four months after final publication in the paper itself in the ASME JOURNAL OF APPLIED MECHANICS.

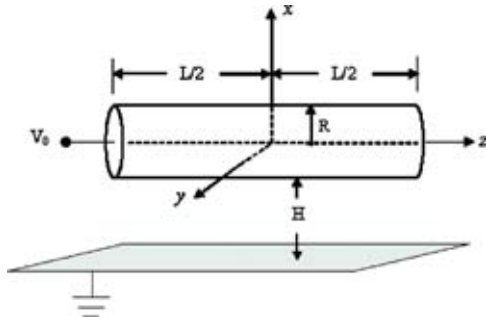


Fig. 1 Schematic of a biased nanotube with radius R and length L above a grounded infinite plane. V is the biased voltage.

For a nanotube with finite length, we used the boundary element method (BEM) to solve the electrostatic governing equations. An image nanotube is considered to computationally remove the infinite plane. The resulting computational domain and boundary conditions are shown in Fig. 2.

The electrostatic potential in the computational domain is given by Poisson equation,

$$\nabla^2 V = 0 \quad \mathbf{r} \in \Omega \quad (2)$$

where V is the potential and Ω is the domain exterior to the conductor and its image. The electric field strength is $\mathbf{E} = -\nabla V$, while the surface charge density is $\rho_A = \epsilon_0 \mathbf{E} \cdot \mathbf{n}$, and \mathbf{n} is the unit vector perpendicular to the surface. The charge density per unit length along the length direction of the nanotube is given by

$$\rho_s = \int_s \rho_A ds, \quad (3)$$

where s is the circumference of the nanotube ($s = 2\pi R$). Note that the above equation only includes charges on the side surfaces. The total electric charge on the nanotube is

$$Q = \oint_A \rho_A dA = \oint_A \epsilon \mathbf{E} \cdot \mathbf{n} dA \quad (4)$$

where A is the total surface area of the nanotube cylinder, which includes the end surfaces.

Results and Discussions

The numerical integration of the above equations is performed using CFD-ACE+, a commercial code from CFD Research Corporation. For consistency, all results are reported for a unitary voltage applied to the nanotube. Also, except for otherwise stated, the radius of the nanotube used in the calculation is $R = 20$ nm, which is common value of multiwalled carbon nanotubes. A spacing between the nanotube and substrate $H = 500$ nm is considered.

One example of the charge distribution on the nanotube is shown in Fig. 3. It is clear that at the end of the nanotube, the charge density is much higher than along its central part, where the charge distribution is almost uniform.

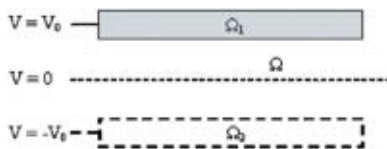


Fig. 2 Side view of the computation domain and boundary conditions for the potential. The middle dotted line represents the infinite plane ($V=0$). Ω_1 and Ω_2 denote the boundaries of the conductor and its image.

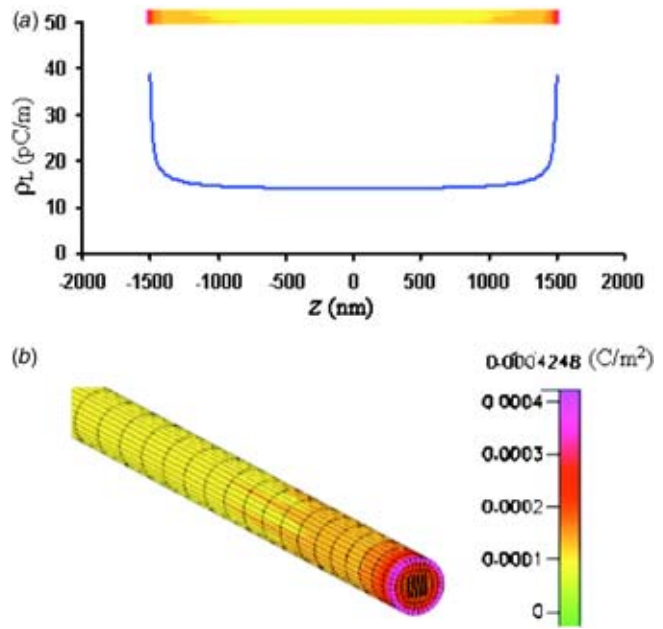


Fig. 3 Plot of charge distribution along a nanotube with length $L = 3000$ nm. (a) Curve showing the charge distribution per unit length on the side surface of the nanotube. (b) Contour plot showing charge distribution per unit area in the neighborhood of the nanotube end. The plot also shows the employed BEM mesh.

The charge per unit length on the side surface of nanotubes with various lengths in the range $L = 1000$ – 4000 nm, are shown in Fig. 4. The dotted line shows the charge per unit length for an infinitely long cylinder, as given by Eq. (1). For $L = 1000$ nm, the charge density in the central part of the cylinder is higher than the result given by Eq. (1), while for $L = 2000, 3000$, and 4000 nm, the charge distribution in the central part gradually approaches the value given by Eq. (1). Likewise, for these cases, the charge distributions at the ends are practically identical. For a given R and H , if $L \gg L^*$, the charge distribution in the central part of the cylinder is uniform and follows Eq. (1). By contrast, the charge distribution at the ends is independent of L . Here L^* is a “characteristic length,” function of R and H , beyond which the distributed charge per unit length along the side surface of the cylinder asymptotically approaches the distributed charge per unit length of a freestanding infinitely long cylinder, ρ_{L0} , which is given by Eq. (1). For $L \gg L^*$, the side surface charge can be expressed as

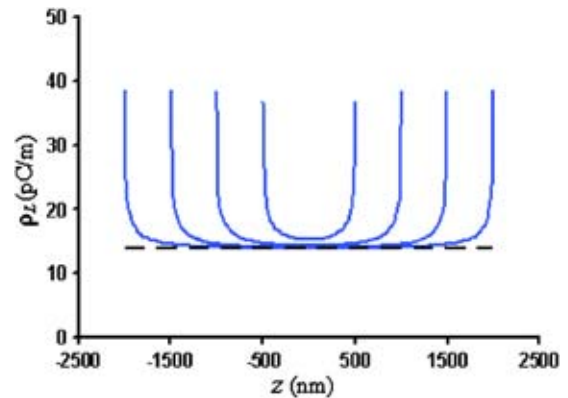


Fig. 4 Charges per unit length on the side surface of nanotubes with different lengths. The horizontal black dash line shows the value given by Eq. (1), i.e., infinitely long nanotube.

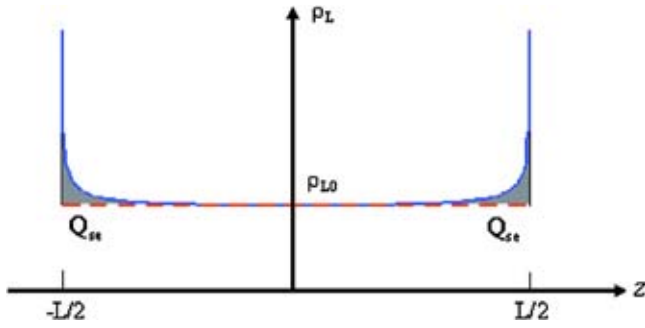


Fig. 5 Charge per unit length on the side surface of nanotube with $L \gg L^*$. The end charge Q_{se} is given by the area between the nonuniform charge distribution curve and the uniform charge distribution corresponding to an infinite tube.

$$Q_s = \rho_{L0}L + 2Q_{se} \quad (5)$$

where $Q_{se} = \int_0^{L/2} (\rho_L - \rho_{L0}) dz$ is the lumped end charge, i.e., the charge in the gray area shown in Fig. 5.

If $L \gg L^*$, the total charges on the surface of the cylinder, including both the charges on the side surface and the two planar end surfaces, is given by

$$Q = Q_s + 2Q_e = \rho_{L0}L + 2(Q_{se} + Q_e) = \rho_{L0}L + 2Q_c \quad (6)$$

where Q_e is the charge on the planar surface at the tube end and Q_c is the concentrated charge on each end of the cylinder as $Q_c = Q_{se} + Q_e$.

Figure 6 shows the total charge as a function of the nanotube length L when $R=20$ nm and $H=500, 1000,$ and 1500 nm, respectively. The corresponding concentrated charge for various nanotube lengths is given in Fig. 7. It can be noticed that the concentrated charge tends to a constant value beyond a certain length L . We define such concentrated charge as $Q_c(\infty)$. In such case $Q_c \approx Q_c(\infty)$, where $Q_c(\infty)$ and L^* can be estimated by the equations given in Appendix A. $Q_c(\infty)$ is plotted as a horizontal line in Fig. 7. Likewise, the value of L^* is represented by the vertical dotted line. Specifically, for $H=500, 1000,$ and 1500 nm, the corresponding characteristic lengths L^* are approximately 2000, 3500, and 4500 nm, respectively.

From this observation, it is inferred that the charge distribution of a finite length nanotube can be modeled with uniform charges distribution corresponding to an infinite nanotube, plus end concentrated charges. Note that the existence of end planes has two effects: (1) there are additional charges on such planes (the corresponding end surface charge is Q_e), and (2) the end plane affects

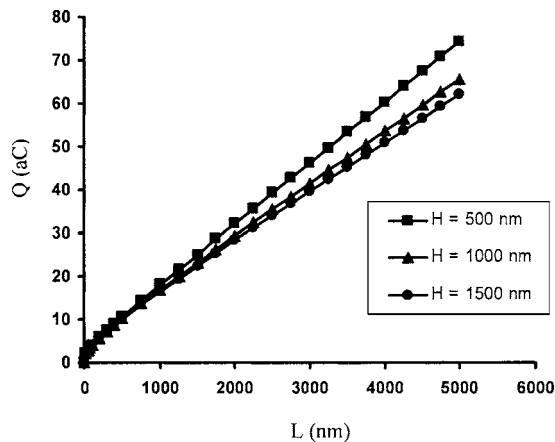


Fig. 6 Total charge Q as a function of tube length L , ranging from 0 to 5000 nm, for $H=500, 1000,$ and 1500 nm, respectively

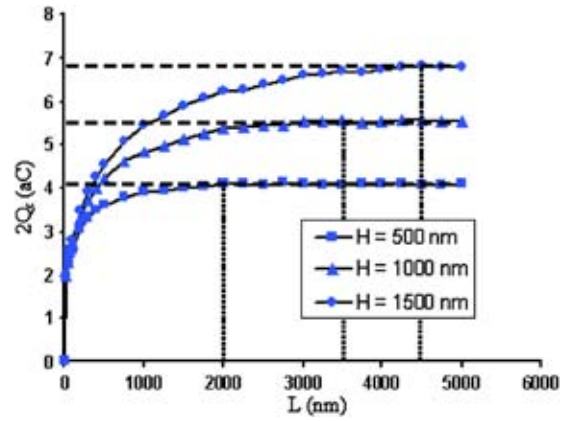


Fig. 7 Concentrated charge at the two ends of the tube ($2Q_c$) for the same case as in Fig. 6

the distribution of the charge along the side surface of the nanotube. The effect is more significant in the area close to the ends than the area in the middle of the nanotube. When the tube is long enough, the charge distribution of the middle part of the tube is not significantly affected by the end surfaces. For the limit case, when the tube becomes infinitely long, the end planes move to $\pm\infty$ and the charge distribution follows Eq. (1). If the length of the nanotube $L < L^*$, the charges per unit length in the central part of the nanotube do not follow Eq. (1), and both Q_s and Q_e are dependent on the length L . In such a case, a nonuniform charge distribution along the whole cylinder must be considered.

For $L \gg L^*$, since the end charge Q_c is independent of the length L , Q_c can be described as a function of R and H , i.e., $Q_c = Q_c(R, H)$. Through a parametric study for $R=10-30$ nm, $H=100-1500$ nm and $L=L^*-5000$ nm (L^* is listed in Table 1) the following formula was identified:

$$Q_c \cong A\rho_{L0}[R(H+R)^2]^{1/3} \quad (7)$$

where A is a constant, which was determined numerically to be $A \approx 0.85$. The values computed for A are given in Table 2.

If we define, $h=H+R$, the distance between the axis of the nanotube and the ground plane, Eq. (10) can be rewritten as $Q_c = A\rho_{L0}(Rh^2)^{1/3}$.

Hence, for $L \gg L^*$, the total charge Q can be written as

$$Q = \rho_{L0}[2A(Rh^2)^{1/3} + L] \cong \rho_{L0}[1.7(Rh^2)^{1/3} + L] \quad (8)$$

For conductive nanotubes or nanowires based NEMS, one or both ends of the nanotube/nanowire are clamped. Figure 8 illustrates a configuration in which a nanotube cylinder is centrally clamped to a box-shaped electrode and biased with respect to an

Table 1 L^* for particular values of the parameters R and H

H(nm) \ R(nm)	L^* (nm)		
	10	20	30
100	300	600	750
250	750	1000	1250
500	1000	2000	3250
1000	2250	3500	4000
1500	4000	4500	4750

Table 2 Constant A in Eq. (10) for particular values of the parameters R and H

H(nm) \ R(nm)	R(nm)		
	10	20	30
100	0.8342	0.8625	0.8671
250	0.8304	0.8452	0.8651
500	0.8307	0.8320	0.8699
1000	0.8521	0.8393	0.8655
1500	0.8646	0.8541	0.8555

infinite plane. A comparison of charge distribution between this case and the case of a free standing nanotube is shown in Fig. 9. The parameters used in the simulation are $R=20$ nm, $H=500$ nm, $L=3000$ nm and the length, width and height of the electrode are $L_e=6000$ nm, $W_e=6000$ nm and $H_e=500$ nm, respectively. From Fig. 9, it is inferred that the clamped end imposes a significant effect to the charge distribution in the region close to it. By contrast, the charge distribution on the free end follows closely the charge distribution corresponding to the free-standing tube (maximum deviation $<6\%$). This finding is consistent with the result reported by Rotkin et al. [13]. The charge distribution on a deflected nanotube cantilever with moderate de-

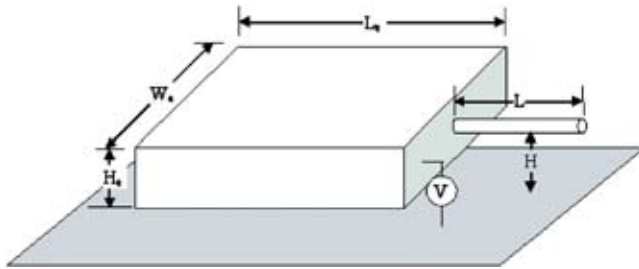


Fig. 8 Schematic of a biased one-end-clamped nanotube cantilever above an infinite plane. The radius of the nanotube cylinder is R.

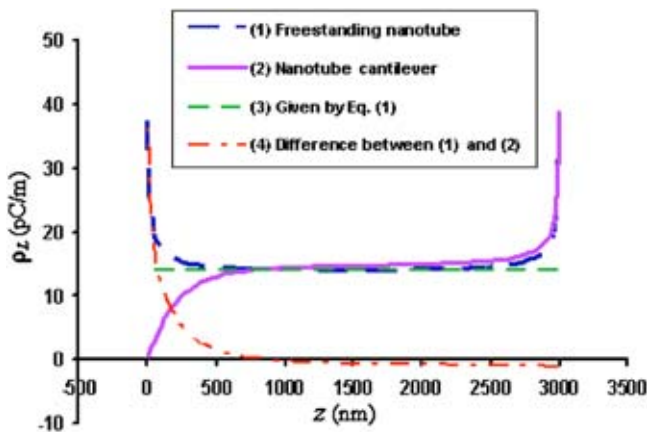


Fig. 9 Comparison of the charge distribution corresponding to a cantilever nanotube and a freestanding nanotube, both of length L. The parameters used in the simulation are $R=20$ nm, $H=500$ nm, $L=3000$ nm.

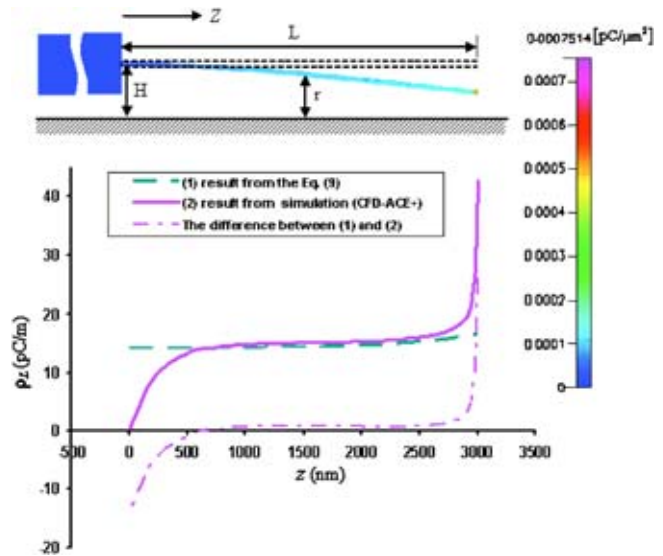


Fig. 10 Plot of charge distribution along a deflected nanotube cantilever. The contour shows the charge distribution per unit area (side view). The plot shows a comparison of the charge distribution per unit length for the deflected nanotube cantilever and the value given by Eq. (9). The parameters used in the simulation are $L=3000$ nm, $R=20$ nm, $H=500$ nm, $r(L)=264$ nm.

flexion is also examined. Figure 10 shows the charge distribution on the same nanotube cantilever as in Fig. 9, with deflection assuming a second polynomial shape; $r=r(z)$ is the distance between the low fiber of the deflected nanotube cantilever and the ground. From Fig. 10, it can be observed that, except for the regions close to the free end and the clamped end, the charge distribution per unit length closely follows the uniform charge distribution given by Eq. (1) with H replaced by $r(z)$ (maximum deviation $<6\%$), that is,

$$\rho_{LD}(z) = \frac{2\pi\epsilon_0 V_0}{a \cosh(1 + r(z)/R)} \quad (9)$$

The difference at the free end shown in Fig. 10 is lumped into a concentrated charge as previously discussed. The concentrated charge at the free end is found to follow Eq. (7) with ρ_{L0} replaced by $\rho_{LD}(L)$.

For electrostatic actuated nanotube cantilevers, the effect of charges present at the clamped end on the deflection of the nanotube is quite limited because the distance for generating a bending moment is small. When calculating the electrostatic force, it is reasonable to assume it is composed of the effect of the uniform charge distribution along the cantilever, plus the effect of the concentrated charge on the free end. Thus,

$$\rho_L(z) \cong \rho_{LD}(z) \{1 + 0.85[R(H+R)^2]^{1/3} \delta(z-L)\} \quad (10)$$

where $\delta(z)$ is the Dirac function. The effect of the concentrated charge on the deflection of the nanotube is substantial. With the consideration of the concentrated charge based on Eq. (10), the pull-in voltage, one of the key parameters for NEMS cantilever devices, was reported to decrease by about 14% with respect to the case in which only a uniform charge distribution is considered [16].

In summary, in this paper the charge distribution on a biased finite length nanotube cylinder, with diameter of 20–60 nm, above an infinite grounded plane is investigated. The relationship between charge distribution and the geometry of nanotubes is studied in detail by classical electrostatics using full 3D numerical simulation based on the boundary element method (BEM). A model of the concentrated charge on the ends of nanotubes is proposed based on a parametric study. A geometric condition for

the validity of the model is assessed based on a characteristic length. The charge distribution of a cantilever nanotube device is also examined. The results here reported are expected to be useful in modeling the electrostatic force exerted on carbon nanotubes and nanowires based NEMS device.

Acknowledgment

The authors acknowledge the support from the FAA through Award No. DTFA03-01-C-00031 and the NSF through award No. CMS-0120866. We would like to express our appreciation to Dr. J. Newcomb and Dr. J. Larsen-Base for supporting this work. Work was also supported in part by the Nanoscale Science and Engineering Initiative of the National Science Foundation under NSF Award No. EEC-0118025. The authors also thank Dr. N. Moldovan and Dr. N. Pugno for helpful discussions.

Appendix

If $\{Q_c^i\}$ is the end charge for tube length $\{L_{ij}, L_{i+1} > L_i, 1 \leq i \leq N\}$. We assume $\{Q_c^i\}$ is converging. If $\forall \varepsilon_1$ and $\exists k, 1 \leq k \leq N-1; \forall m \geq k |Q_c^{m+1} - Q_c^m| \leq \varepsilon_1$

$$Q_c(\infty) = \frac{\sum_{j=k}^N Q_c^j}{N - k + 1}$$

If $\forall \varepsilon_2$ and $\exists k, 1 \leq k \leq N; \forall m \geq k |Q_c^m - Q_c(\infty)| \leq \varepsilon_2$

$$L^* = L_{\min(k)}$$

For practical reason, $\varepsilon_1 = \varepsilon_2 = Q_c^N / 100$.

References

[1] Akita, S., Nakayama, Y., Mizooka, S., Takano, Y., Okawa, T., Miyatake, Y., Yamanaka, S., Tsuji, M., and Nosaka, T., 2001, "Nanotweezers Consisting of

Carbon Nanotubes Operating in an Atomic Force Microscope," *Appl. Phys. Lett.*, **79**, pp. 1691–1693.
 [2] Kim, P., and Lieber, C. M., 1999, "Nanotube Nanotweezers," *Science*, **126**, pp. 2148–2150.
 [3] Rueckes, T., Kim, K., Joslevich, E., Tseng, G. Y., Cheung, C., and Lieber, C. M., 2000, "Carbon Nanotube-Based Nonvolatile Random Access Memory for Molecular Computing," *Science*, **289**, pp. 94–97.
 [4] Kinaret, J., Nord, T., and Viefers, S., 2003, "A Carbon-Nanotube-Based Nanorelay," *Appl. Phys. Lett.*, **82**, pp. 1287–1289.
 [5] Fennimore, M., Yuzvinsky, T. D., Han, W. Q., Fuhrer, M. S., Cummings, J., and Zettl, A., 2003, "Rotational Actuator Based on Carbon Nanotubes," *Nature (London)*, **424**, pp. 408–410.
 [6] Ke, C.-H., and Espinosa, H. D., 2004, "Feedback Controlled Nanocantilever NEMS Device," *Appl. Phys. Lett.*, **85**, pp. 681–683.
 [7] Husain, A., Hone, J., Postma, H. W. Ch., Huang, X. M. H., Drake, T., Barbic, M., Scherer, A., and Roukes, M. L., 2003, "Nanowire-Based Very-High-Frequency Electro-Mechanical Resonator," *Appl. Phys. Lett.*, **83**, pp. 1240–1242.
 [8] Ziegler, K. J., Lyons, D. M., Holmes, J. D., Erts, D., Polyakov, B., Olin, H., Svensson, K., and Olsson, E., 2004, "Bistable Nanoelectromechanical Devices," *Appl. Phys. Lett.*, **84**, pp. 4074–4076.
 [9] Dequesnes, M., Rotkin, S. V., and Aluru, N. R., 2002, "Calculation of Pull-in Voltage for Carbon-Nanotube-Based Nanoelectromechanical Switches," *Nanotechnology*, **13**, pp. 120–131.
 [10] Lou, L., Nordlander, P., and Smalley, R. E., 1995, "Fullerene Nanotube in Electric Fields," *Phys. Rev. B*, **52**, pp. 1429–1432.
 [11] Krcmar, M., Saslow, W. M., and Zangwill, A., 2003, "Electrostatic of Conducting Nanocylinder," *J. Appl. Phys.*, **93**, pp. 3495–3500.
 [12] Bulashevich, K. A., and Rotkin, S. V., 2002, "Nanotube Devices: A Microscopic Model," *JETP Lett.*, **75**, pp. 205–209.
 [13] Rotkin, S. V., Shrivastava, V., Bulashevich, K. A., and Aluru, N. R., "Atomic Capacitance of a Nanotube Electrostatic Device," 2002, *Int. J. Nanosci.*, **1**, pp. 337–346.
 [14] Keblinski, P., Nayak, S. K., Zapol, P., and Ajayan, P. M., 2002, "Charge Distribution and Stability of Charged Carbon Nanotube," *Phys. Rev. Lett.*, **89**, 255503.
 [15] Hayt, W., and Buck, J., 2001, *Engineering Electromagnetics*, 6th ed. McGraw-Hill, New York.
 [16] Ke, C.-H., Espinosa, H. D., and Pugno, N., 2005, "Numerical Analysis of Nanotube Based NEMS Devices—Part II: Role of Finite Kinematics, Stretching and Charge Concentration," *ASME J. Appl. Mech.*, **72**, pp. 726–731.